C_6H and C_6D: Electronic spectra and Renner-Teller analysis

Dongfeng Zhao (赵东锋),[1,a)] Mohammad Ali Haddad,[1] Harold Linnartz,[1,2] and Wim Ubachs[1]

[1]*Institute for Lasers, Life, and Biophotonics, VU University Amsterdam, De Boelelaan 1081, NL 1081HV Amsterdam, The Netherlands*

[2]*Sackler Laboratory for Astrophysics, Leiden Observatory, University of Leiden, PO Box 9513, NL 2300 RA Leiden, The Netherlands*

(Received 16 May 2011; accepted 18 June 2011; published online 26 July 2011)

Rotationally resolved spectra of the $B^2\Pi$ - $X^2\Pi$ 0_0^0 electronic origin bands and 11_1^1 $\mu^2\Sigma$ - $\mu^2\Sigma$ vibronic hot band transitions of both C_6H and C_6D have been recorded in direct absorption by cavity ring-down spectroscopy through a supersonically expanding planar plasma. For both origin and hot bands accurate spectroscopic parameters are derived from a precise rotational analysis. The origin band measurements extend earlier work and the 11_1^1 $\mu^2\Sigma$ - $\mu^2\Sigma$ vibronic hot bands are discussed here for the first time. The Renner-Teller effect for the lowest bending mode ν_{11} is analyzed, yielding the Renner parameters ε_{11}, vibrational frequencies ω_{11}, and the true spin-orbit coupling constants A_{SO} for both $^2\Pi$ electronic states. From the Renner-Teller analysis and spectral intensity measurements as a function of plasma jet temperature, the excitation energy of the lowest-lying 11_1 $\mu^2\Sigma$ vibronic state of C_6H is determined to be (11.0 ± 0.8) cm^{-1}. © *2011 American Institute of Physics*. [doi:10.1063/1.3609112]

I. INTRODUCTION

The hextriynyl radical C_6H, a member of the linear carbon chain $C_{2n}H$ series, is an important intermediate in interstellar chemistry. It was initially detected by radio astronomy in the cold dense cloud TMC-1,[1,2] and later unambiguously identified in a laboratory microwave study.[3] In the latter study accurate spectroscopic constants for the $X^2\Pi$ electronic ground state were derived that allowed further identifications in TMC-1[4] and around the carbon-rich star IRC+10216.[2,5–8] Following matrix isolation studies[9] and the improvement in detection sensitivity of optical spectroscopic techniques (see e.g. Refs. 10 and 11), it became possible to record the electronic spectra of C_6H,[12–15] among many other carbon chain radicals. In a combined microwave and optical study[16] the rotationally fully resolved origin band spectra of the $B^2\Pi$ - $X^2\Pi$ electronic system of C_6H and C_6D were analyzed, resulting in accurate spectroscopic parameters for both $^2\Pi$ states.

Recently, the detection of C_6H^-, the first interstellar anion,[17] and vibrationally excited C_6H[18,19] has renewed the spectroscopic and astronomical interest in the hextriynyl radical. In Ref. 19, a detailed laboratory microwave study of an excited C_6H and C_6D bending vibrational level ($\nu_{11} = 1$) has been reported for two vibronic states, $^2\Sigma$ and $^2\Delta$. The resulting effective spectroscopic parameters in combination with the very low excitation energy (~20 K) of the $\mu^2\Sigma$ vibronic component are indicative for a relatively strong Renner-Teller interaction, i.e., the coupling between the bending vibrational and degenerate electronic orbital angular momenta, for the ν_{11} mode in the $X^2\Pi$ state.

In the present work, an extended analysis is presented for the $B^2\Pi$ - $X^2\Pi$ 0_0^0 origin band transitions of C_6H and C_6D. The focus, however, is on the rotationally resolved 11_1^1 $\mu^2\Sigma$ - $\mu^2\Sigma$ vibronic hot band transition that is presented here for the first time. The Renner-Teller (R-T) analysis for the lowest bending mode ν_{11} is carried out. The precise excitation energy of the 11_1 $\mu^2\Sigma$ state follows from the R-T analysis and from experimental data on band intensities.

II. EXPERIMENTAL DETAILS

The C_6H and C_6D radicals are produced (among other species) in a supersonically expanding plasma by discharging a mixture of acetylene in helium. The spectra are recorded in direct absorption using cavity ring-down spectroscopy and details of the setup and experimental procedures are available from Refs. 20–22. A 3 cm × 100 μm slit discharge nozzle is employed to generate a planar plasma expansion which provides an essentially 'Doppler-free' environment and a relatively long effective absorption path length. Three gas mixtures, ~0.5% C_2H_2/He, ~0.3% C_2D_2/He, and ~(0.2% C_2H_2 + 0.2% C_2D_2)/He, are used in the present experiment to create a C/H, C/D, and C/H/D containing plasma, respectively. Typical running conditions are: V/I ≈ −750 V/100 mA and ~10 bar backing pressure. The nozzle is mounted with its slit parallel to and a few mm away from the optical axis between two highly reflective mirrors that form an optical cavity with a total length of 58 cm. Cavity ring-down spectroscopy is used to measure spectra in direct absorption. The tunable output of a pulsed Nd:YAG pumped dye laser system (10 Hz) is injected into the cavity and the light leaking out is detected by a photo-multiplier visualizing separate ring-down events. Typical ring-down times are and amount to 60–80 μs. A spectrum is subsequently obtained by measuring the ring-down time as a function of laser frequency. Laser bandwidths of better than 0.035 cm^{-1} are obtained by running the dye laser in a 2nd

a)Author to whom correspondence should be addressed. Electronic mail: d.zhao@vu.nl.

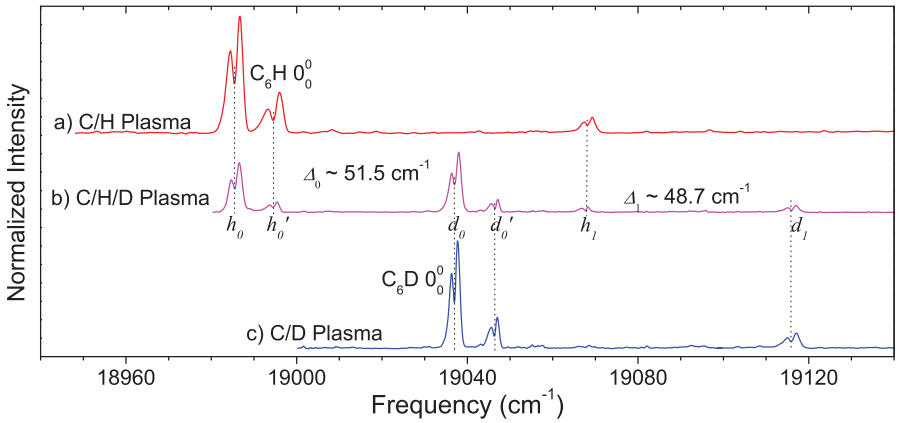

FIG. 1. Experimentally observed spectra through: (a) C/H plasma, (b) mixed C/H/D plasma, and (c) C/D plasma. The vertical dotted lines indicate the band origins of the observed bands. Δ denotes the isotopic shift.

order grating setting, as recently demonstrated in the study of HC_7H.[21] An absolute frequency calibration with accuracy better than 0.02 cm^{-1} is realized by recording simultaneously an iodine reference spectrum and an etalon to correct for the non-linear scanning of the dye laser.

In addition to the slit nozzle experiments spectra are recorded using a pinhole discharge nozzle, which has been described in detail previously.[22] The best achievable resolution with this nozzle is less, but spectra with different rot-vibrational temperatures can be more easily obtained by varying the distance of pinhole nozzle orifice to the cavity axis. Specifically, for the C_6H radical studied in the present experiment, spectra are obtained at six different distances between 15 and 2 mm resulting in rotational temperatures between ~7 and 21 K.

III. RESULTS AND ANALYSIS

A. Observed spectra

In Ref. 14 an optical survey of hot electronic spectra of C_6H was presented using cavity ring-down spectroscopy in a hollow cathode discharge of acetylene and helium. These spectra were not rotationally resolved as a consequence of the high rotational (and vibrational) temperature >200 K (yielding band heads) and Doppler broadening in the cell. Only the C_6H 0_0^0 bands were unambiguously identified, following matrix work.[12,13] The focus of the present experiment is a high resolution study of vibronic hot transitions starting from the low-lying excited vibrations of C_6H (C_6D) and to link the optical spectra to recent microwave work.[19]

Figure 1 shows overview spectra recorded through an expanding hydrocarbon plasma. Three absorption bands, labeled [h_0], [h_0'], and [h_1], are observed in C/H plasma, as well as the corresponding D-isotopic bands (labeled [d_0], [d_0'] and [d_1]) in C/D plasma. These six bands are also visible in the mixed C/H/D plasma.

Following previous work,[14,16] the band pairs [h_0, h_0'] and [d_0, d_0'] can be unambiguously assigned to $B^2\Pi_\Omega$ - $X^2\Pi_\Omega$ (Ω = 3/2 - 3/2 and 1/2 - 1/2) 0_0^0 electronic origin band transitions of C_6H and C_6D, respectively. The fully resolved spectra of these bands are shown in Figs. 2 and 3. The spectra are very similar to the ones previously presented in Ref. 14. The lower detection limit and the better laser

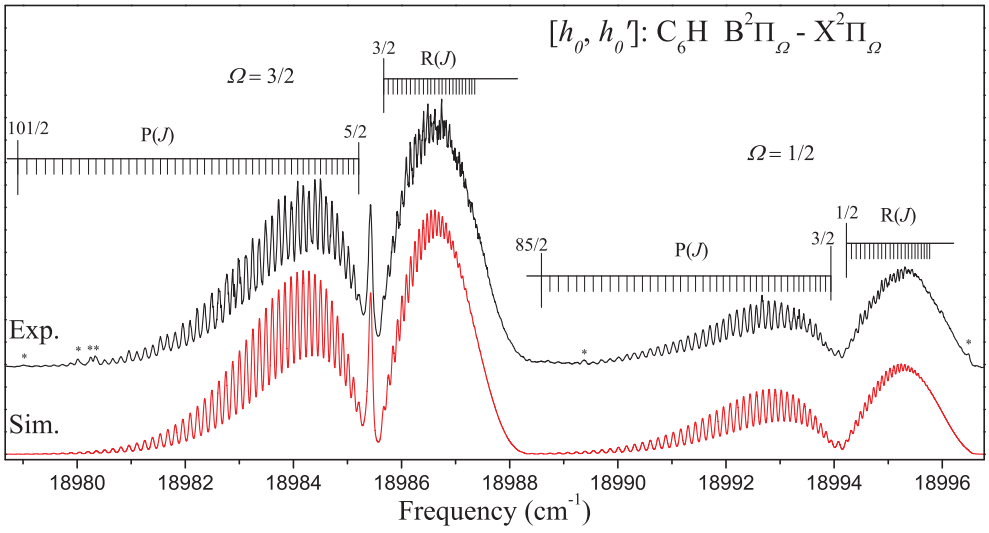

FIG. 2. The rotationally resolved spectrum of the $B^2\Pi - X^2\Pi$ 0_0^0 electronic origin transition of C_6H, corresponding to the band pair [h_0, h_0'] in Fig. 1. The simulated spectrum for a rotational temperature of ~21 K is shown in the lower trace. The irregular features marked with an asterisk are due to blending transitions by other small species like C_2, CH, etc.

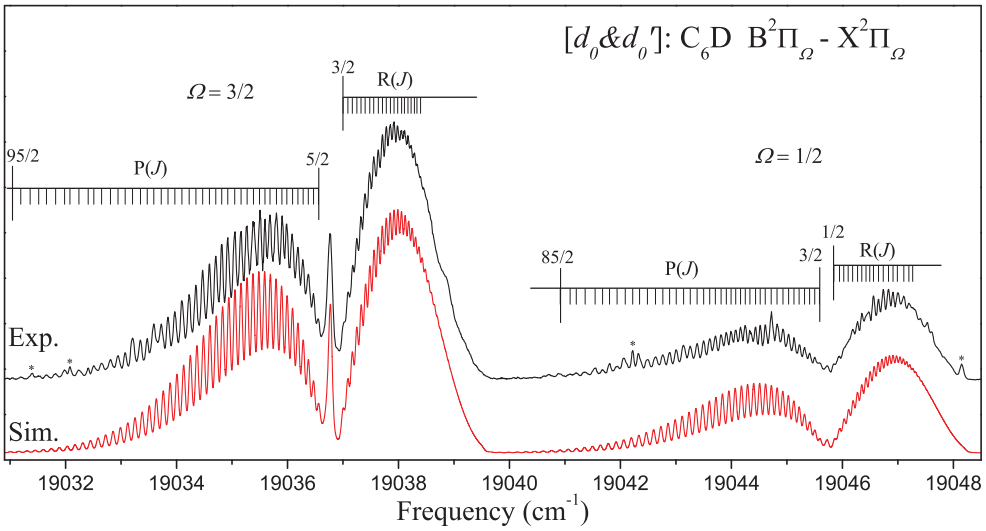

FIG. 3. The rotationally resolved spectrum of the $B^2\Pi - X^2\Pi$ 0_0^0 electronic origin transition of C_6D, corresponding to the band pair [d_0, d_0'] in Fig. 1. The simulated spectrum for a rotational temperature of ~21 K is shown in the lower trace. The irregular features marked with an asterisk are due to blending transitions of other small species like C_2, CD, etc.

bandwidth in the present experiment allow the recording of higher J-value transitions (see the supplementary material[23]), and to derive more accurate values for the spectroscopic constants T_0, B', and A'. The parameter set can be extended with a centrifugal distortion constant D' and spin-rotational constant γ' for the excited state. The fit[24] is performed using the PGOPHER software[25] and the resulting values are listed in Table I.

The band [h_1] observed in the C/H plasma and the band [d_1] observed in the C/D plasma have not been reported before and are discussed here in detail. The newly observed band [h_1] coincides with more than three absorption peaks recorded in the hollow cathode discharge.[14] The assignment of the bands [h_1] and [d_1] to vibrationally excited C_6H and C_6D, therefore, is logical and consistent with a number of observations:

(i) As shown in Figs. 4 and 5, the rotational contours of the bands [h_1] and [d_1] are almost the same. The corresponding isotopic shift is ~49 cm^{-1}, and this value is very close to the isotopic shift (~52 cm^{-1}) of the 0_0^0 electronic origin bands ([h_0, h_0'] versus [d_0, d_0']) of C_6H and C_6D, respectively. This indicates that [d_1] represents the D-isotopically shifted band of [h_1]

(ii) No additional bands between or around [h_1] and [d_1] are observed in the C/H/D plasma (see Fig. 1), indicating that the carrier must be of the form C_nH with only one H/D atom.

TABLE I. Spectroscopic constants (in cm^{-1}) of C_6H and C_6D.

	C_6H $B^2\Pi$ - $X^2\Pi$		C_6D $B^2\Pi$ - $X^2\Pi$	
	0_0^0	11_1^1 $\mu^2\Sigma$ - $\mu^2\Sigma$	0_0^0[a]	11_1^1 $\mu^2\Sigma$ - $\mu^2\Sigma$
A''[b]	−15.0424		−15.1276	
B''[b]	0.04640497	0.04652018	0.04429243	0.0443852
$D''(10^{-9})$[b]	1.35	1.55	1.20	1.38
$\gamma''(10^{-3})$[b]	−7.12	−0.628	−3.85	−0.631
T[c]	18989.7672(4)	19066.8372(6)	19041.2564(5)	19115.5251(10)
A'	−23.6924(7)		−24.0727(10)	
B'	0.0455952(5)	0.0456873(11)	0.0435921(39)	0.0436478(19)
$D'(10^{-9})$	1.58(28)	39.1(1.2)	1.20[d]	13.4(1.7)
$\gamma'(10^{-3})$	−3.63(18)	38.29(6)	−6.3(7)	39.68(10)
B''/B'[e]	1.0177	1.0182	1.0171	1.0171
B_0''/B_{eff}''[e]	0.9975		0.9979	
B_0'/B_{eff}'[e]	0.9980		0.9979	

[a]Spectroscopic constants are obtained by fitting rotational transitions with $J' \leq 15.5$ for the $\Omega = 3/2$ component and $J' \leq 10.5$ for the $\Omega = 1/2$ component.[24]

[b]Spectroscopic constants for the lower states are taken from Refs. 16 and 19 and fixed.

[c]The errors of the band origins (T) represent the statistical uncertainties as obtained from the least squares fit. The maximum uncertainty of the absolute laser frequency in the present work is ~0.02 cm^{-1}.

[d]Fixed parameter in the least-squares fit.

[e]Ratio of rotational constants is dimensionless.

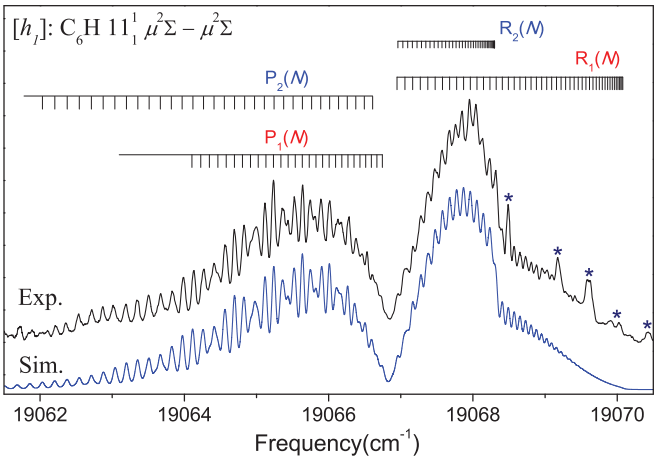

FIG. 4. The rotationally resolved spectrum of the 11_1^1 $\mu^2\Sigma$- $\mu^2\Sigma$ vibronic transition of C_6H, corresponding to band [h_1] in Fig. 1. The simulated spectrum for a rotational temperature of ~21 K is shown in the lower trace. The irregular features marked with an asterisk are due to blending transitions by other small species.

(iii) As shown in Figs. 4 and 5, doublet P- and R-branch contours with large spin-splitting, i.e., $P_1(N)$-$P_2(N)$, and $R_1(N)$-$R_2(N)$, can be seen in the rotationally resolved spectra of [h_1] and [d_1]. In contradiction to the origin band transitions (Figs. 2 and 3) no Q-branch is present. This is typical for a $^2\Sigma$ - $^2\Sigma$ transition of a linear molecule.

(iv) From the combination differences, R(N-1) - P(N+1) = $B''(4N+2)$, the approximate rotational constant B'' for the lower $^2\Sigma$ state is estimated as ~0.05 cm^{-1}. This deviates substantially from B'' values found for $C_5H^{(+/-)}$ (~ 0.08 cm^{-1})[26,27] and $C_7H^{(+/-)}$ (~0.03 cm^{-1}),[28] but is of the same magnitude as that of $C_6H^{(+/-)}$ (~0.05 cm^{-1}).[19] Since electronic spin multiplicities for the C_6H^+ and C_6H^- are triplet and singlet, respectively, C_6H remains as only candidate.

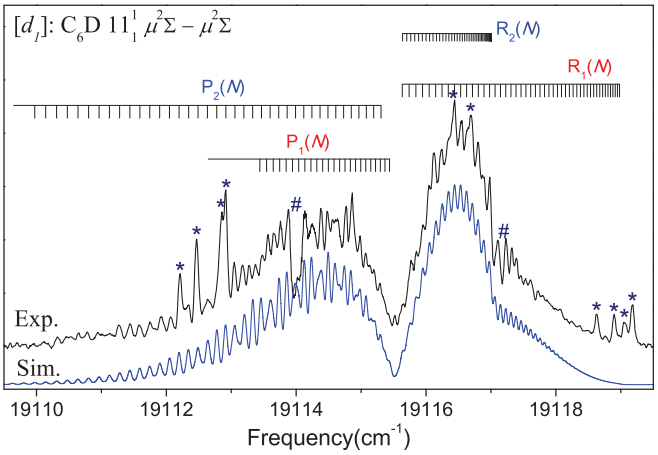

FIG. 5. The rotationally resolved spectrum of the 11_1^1 $\mu^2\Sigma$- $\mu^2\Sigma$ vibronic transition of C_6D, corresponding to the band [d_1] in Fig. 1. The simulated spectrum for a rotational temperature of ~21 K is shown in the lower trace. The irregular features marked with an asterisk are due to blending transitions by other small species. The irregular features marked with a hash are reproducible, and may be due to a local perturbation in the upper state.

(v) The lowest $\mu^2\Sigma$ vibronic state of C_6H, which is split from the ν_{11} vibrational levels due to the R-T effect, was estimated in a recent microwave experiment[19] to be only ~14 ± 7 cm^{-1} above the $X^2\Pi_{3/2}$ level. In a plasma expansion such a low-lying state is sufficiently populated to be observable.

These observations hint at an assignment of the observed [h_1] and [d_1] bands to transitions starting from a vibrationally excited level of C_6H and C_6D. Since no other bands are observed besides the electronic origin transition of C_6H/C_6D, the vibrational mode exited in the upper state is likely the same ν_{11} bending mode. Thus, summarizing, the most likely assignment of the bands [h_1] and [d_1] is the 11_1^1 $\mu^2\Sigma$ - $\mu^2\Sigma$ vibronic hot band transitions of C_6H and C_6D, respectively. An unambiguous proof is given in Sec. III B, where it is shown, that the new bands [h_1] and [d_1] can be fitted using the lower ν_{11} $\mu^2\Sigma$ vibronic state constants of C_6H and C_6D as derived in Ref. 19.

B. Rotational analysis

As shown in Figs. 4 and 5, both bands [h_1] and [d_1] exhibit four main branches, $R_1(N)$ and $R_2(N)$, $P_1(N)$ and $P_2(N)$, consisting of transitions with $\Delta N = \pm 1$, respectively. Most rotational transitions between the doublet P- and R-branches, particularly in the band origin regions are blended. This blending increases the uncertainty of the transition frequency determinations, particularly for the R_2-branch, compared to the 0_0^0 electronic origin band. The measured line positions for the (partially) resolved rotational transitions of [h_1] and [d_1] are summarized in the supplementary material.[23] All these transition frequencies are included in a least-squares fitting routine for a $^2\Sigma$ - $^2\Sigma$ transition. The rotational levels in both lower and upper $^2\Sigma$ states are described by Hund's case (b) expressions:

$$F_1(^2\Sigma, N) = T_\Sigma + [B_{eff} - DN(N+1)]N(N+1) + \frac{\gamma_{eff}}{2}N \quad (1)$$

$$F_2(^2\Sigma, N) = T_\Sigma + [B_{eff} - DN(N+1)]N(N+1) - \frac{\gamma_{eff}}{2}(N+1) \quad (2)$$

where B_{eff} is the effective rotational constant, D is the centrifugal distortion constant, and γ_{eff} is an effective spin splitting constant, which does not necessarily correspond to the spin-rotational constant in an isolated $^2\Sigma$ state. In the case of a sufficiently large R-T effect, as derived by Hougen,[29] the parameter γ_{eff} depends on the magnitude of the R-T interaction relative to the spin-orbit (SO) interaction in the $^2\Pi$ electronic state. Such an effective spin splitting constant generally has a value of $0 \leq \gamma_{eff} \leq 2B_{eff}$. Its value is close to zero when the R-T interaction is large, and approaches a value of $2B_{eff}$ when the R-T interaction is very small. For the lower ν_{11} $\mu^2\Sigma$ vibronic state of C_6H/C_6D, the R-T effect is relatively large, as has been discussed in Ref. 19. This state can be analyzed separately using the standard rotational Hamiltonian

for an isolated $^2\Sigma$ state. Consequently, the value of the effective spin splitting constant γ_{eff}'' is predominantly determined by the spin-rotational interaction. Large spin splittings in the doublet branch structure of the bands $[h_1]$ and $[d_1]$ predict a smaller R-T effect in the upper state, and the constant γ_{eff}' is most likely determined by a joint SO and R-T interaction.

The least-squares fits are performed using the PGOPHER software.[25] The spectroscopic constants, B_{eff}'', D'', and γ_{eff}'', in the lower ν_{11} $\mu^2\Sigma$ states of C_6H and C_6D for the bands $[h_1]$ and $[d_1]$, are taken from Ref. 19 and fixed, while the band origin T, and spectroscopic constants B_{eff}', D', and γ_{eff}' in the upper $^2\Sigma$ state are set as variable parameters.

The fit results are listed in Table I. The resulting simulated spectra for both bands $[h_1]$ and $[d_1]$ are shown in Figs. 4 and 5. It is found that very characteristic features, such as spectral interferences between P_1-and P_2-branches, and a sharp decrease in intensity around 19068 (19117) cm^{-1} due to the R_2-branch band head are well reproduced in the C_6H (C_6D) simulated spectra.

The derived rotational constants in the upper $\mu^2\Sigma$ states are compared to the constants in the $B^2\Pi$ - $X^2\Pi$ 0_0^0 electronic origin bands of C_6H and C_6D. The change of the rotational constants upon electronic or vibrational excitation reflects the difference of the overall length of the chain. Two sets of rotational constant ratios, B''/B' for the $B^2\Pi$ - $X^2\Pi$ electronic excitation, and $B_0/B_{eff}(^2\Sigma)$ for the vibrational excitation in the same electronic state, are compared in Table I. The similar value of the four B''/B' ratios, ~1.017, agrees with the assumption that the electronic excitation for bands $[h_1]$ and $[d_1]$ is the same as that for the 0_0^0 band of C_6H and C_6D, i.e., $B^2\Pi$ - $X^2\Pi$. The value indicates that the overall length of C_6H and C_6D somewhat increases upon electronic excitation. The similar value of the $B_0''/B_{eff}''(^2\Sigma)$ and $B_0'/B_{eff}'(^2\Sigma)$ ratios of C_6H and C_6D indicates that the excited vibrational mode in both lower and upper electronic state is the same, i.e., the ν_{11} bending vibration. The value of $B_0/B_{eff}(^2\Sigma)$ is ~0.2% smaller than unity and due to the fact that the effective chain length of a linear polyatomic molecule slightly decreases upon excitation of a bending vibration.

C. Renner-Teller analysis

Owing to the R-T interaction, each bending fundamental mode in a $^2\Pi$ electronic state is split into one $^2\Delta$ and two $^2\Sigma$ vibronic states. An effective Hamiltonian that considers both the R-T effect and the SO coupling is required to reproduce the vibronic structure in degenerated $^2\Pi$ electronic states of C_6H. The effective Hamiltonian without the rotational part is expressed as

$$H = H_{vib} + H_{RT} + H_{SO} \tag{3}$$

where H_{vib} is the vibrational Hamiltonian for the bending mode, H_{RT} the R-T Hamiltonian, and H_{SO} the SO coupling term. Because only the lowest bending vibration ν_{11} is considered, the analysis here is simplified by following the assumption that high-order and intermode interactions can be neglected. The representation of the Hamiltonian in Eq. (3) is constructed by a basis set of[30]

$$|\Lambda, v, K, \Sigma\rangle \tag{4}$$

where $\Lambda = \pm 1$ for a $^2\Pi$ state, electronic spin $\Sigma = \pm 1/2$, and $K = |\Lambda + l| = 0$, 1, and 2 corresponding to the Σ, Π and Δ vibronic states, respectively. The non-zero matrix elements of the Hamiltonian in Eq. (3) are[30]

$$\langle v|\, H_{vib}\, |v\rangle = \omega\,(v+1) \tag{5}$$

$$\langle -1, v, K|\, H_{RT}\, |+1, v-2, K\rangle = \frac{\varepsilon\omega}{4}\sqrt{(v-1+K)\,(v+1+K)} \tag{6}$$

$$\langle +1, v, K|\, H_{RT}\, |-1, v-2, K\rangle = \frac{\varepsilon\omega}{4}\sqrt{(v-1-K)\,(v+1-K)} \tag{7}$$

$$\langle +1, v, K|\, H_{RT}\, |-1, v, K\rangle = \frac{\varepsilon\omega}{2}\sqrt{(v+1)^2 - K^2} \tag{8}$$

$$\langle \Lambda, \Sigma|\, H_{SO}\, |\Lambda, \Sigma\rangle = A_{SO}\,\Lambda\,\Sigma \tag{9}$$

where ω is the vibrational frequency of the bending mode, ε the Renner parameter and A_{SO} the true SO splitting constant.

The previous microwave studies[16,19] have resulted in effective spin splittings in the $X^2\Pi$ ground state of C_6H: $A_0''(0_0\ ^2\Pi) \sim -15.04\ cm^{-1}$, and $A_\Delta''(11_1\ ^2\Delta) \sim -11.90\ cm^{-1}$, as well as $A_0'(0^0\,^2\Pi) \sim -23.69\ cm^{-1}$ in the $B^2\Pi$ state. However, to reproduce the vibronic structure in both $^2\Pi$ electronic states knowledge of the vibrational frequencies (ω_{11}'' and ω_{11}') of the ν_{11} bending mode is still required. Considering that the $B_0''/B_{eff}''(\nu_{11})$ ratio is almost the same as $B_0'/B_{eff}'(\nu_{11})$, we assume that

$$0.9\omega_{11}'' \le \omega_{11}' \le 1.1\omega_{11}'' \tag{10}$$

Under this assumption, the parameters ε_{11}, ω_{11} and A_{SO} for both $^2\Pi$ electronic states are fitted using the transition energies of the bands $[h_0]$, $[h_0']$ and $[h_1]$ listed in Table I. The resulting parameters from the R-T analysis are summarized in Table II. The derived vibrational frequency ω_{11} ~95 cm^{-1} is in good agreement with the previously predicted values from theoretical calculations.[31–33] The schematic diagram in Fig. 6 shows the vibronic structures of C_6H derived from the R-T analysis, where the corresponding transitions to the bands $[h_0]$, $[h_0']$ and $[h_1]$ are indicated as well.

The large value for the Renner parameter ε_{11}'' (~0.995) indicates that the potential surface of the $X^2\Pi$ ground state has an energy minimum in a non-linear geometry due to strong coupling between vibrational and electronic orbital angular momenta. Further, the R-T analysis shows that, for such a large ε value the $0_0\ ^2\Pi_{1/2}$ level is significantly mixed with the $11^2\,^2\Pi_{1/2}$ levels. This behavior has also been found for the $A^2\Pi$ state of C_4H,[34] which has a similar electronic configuration and a similarly large Renner parameter (ε ~0.99) as the $X^2\Pi$ state of C_6H.

TABLE II. Vibronic parameters of C_6H and C_6D in both $^2\Pi$ states.

	C_6H		C_6D	
	$B^2\Pi$	$X^2\Pi$	$B^2\Pi$	$X^2\Pi$
ε_{11}[a]	0.08869(2)	0.995(5)	0.08852	0.99(1)[b]
ω/cm^{-1}	95(1)	100(10)	92[c]	97[c]
A_{so}/cm^{-1}	−23.74(1)	−47.5(3)	−24.12[d]	−47

[a]The sign of the parameter ε_{11} could not be unambiguously determined in the present study.
[b]Estimated value.
[c]Vibrational frequencies estimated by $\omega_D/\omega_H \approx (B_D/B_H)^{1/2}$.
[d]Assume $A_{SO}' \approx A_0'$ in C_6D.

In contrast, the R-T effect for the ν_{11} bending mode in the $B^2\Pi$ state of C_6H is much smaller ($\varepsilon' \sim 0.09$) than in the $X^2\Pi$ ground state. According to Hougen, the values of B_{eff} and γ_{eff} for $^2\Sigma$ vibronic states can be approximately expressed by[29,35]

$$B_{eff}^{\mu/k} = B\left(1 \pm \frac{A_{SO}^2 B}{A_\Sigma^3}\right) \tag{11}$$

$$\gamma_{eff}^{\mu/k} = 2B\left(1 - \frac{2\varepsilon\omega}{A_\Sigma} \pm \frac{A_{SO}^2 B}{A_\Sigma^3}\right) \tag{12}$$

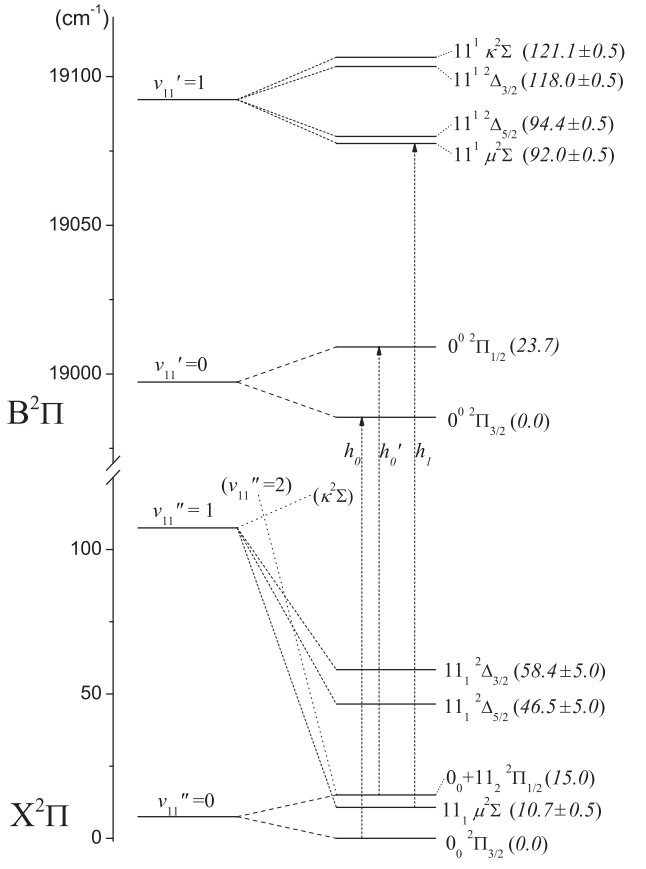

FIG. 6. Schematic diagram of the vibronic structure in both $^2\Pi$ electronic states of C_6H derived from the R-T analysis. The relative energies (in cm^{-1}) with respect to the $v = 0$ $^2\Pi_{3/2}$ level in each electronic state are indicated by italic numbers in brackets.

TABLE III. Spin-orbit coupling constants and Renner parameters of C_6H and C_4H.

	C_6H		C_4H	
	$B^2\Pi$	$X^2\Pi$	$B^2\Pi$[a]	$A^2\Pi$[b]
A_0/cm^{-1}	−23.69	−15.04	−14.8	−28
A_{SO}/cm^{-1}	−23.74	−47.5	−22.1	−45.5
$\lvert\varepsilon_{(CCC\ bending)}\rvert$	$\lvert\varepsilon_{11}\rvert \sim 0.089$	$\lvert\varepsilon_{11}\rvert \sim 0.995$	$\lvert\varepsilon_7\rvert \sim 0.016$	$\lvert\varepsilon_7\rvert \sim 0.061$
$\lvert\varepsilon_{(CCH\ bending)}\rvert$	–	–	$\lvert\varepsilon_6\rvert \sim 0.657$	$\lvert\varepsilon_6\rvert \sim 0.99$

[a]Values taken from Ref. 38.
[b]Values taken from Ref. 34.

where A_Σ is the effective spin splitting between the two $^2\Sigma$ states:

$$A_\Sigma = \sqrt{A_{SO}^2 + 4\varepsilon^2\omega^2} \tag{13}$$

In the case of the 11^1 $\mu^2\Sigma$ vibronic state of C_6H, using the values of $B' \approx B_{eff}'$, ε', ω_{11}', and A_{SO}' listed in Tables I and II, we obtain $\gamma_{eff}' \approx 0.0386$ cm^{-1}, which is in good agreement with the $\gamma_{eff}' = 0.038285$ cm^{-1} as derived from the rotational analysis on band $[h_1]$.

Since the microwave data for the 11_1 $^2\Delta$ vibronic state of C_6D have not been reported up to now, it remains a challenge to reproduce the vibronic structure of C_6D. Using γ_{eff}' ~ 0.0399 cm^{-1} in the 11^1 $\mu^2\Sigma$ vibronic state of C_6D, the parameter ε_{11}' can be estimated to be ~ 0.0885 from Eqs. (11)–(13). Since the R-T effect in the ground state of C_6H is very large, it is expected that the vibronic structure of C_6D in the low energy range (<100 cm^{-1}) may be very similar to that in the $X^2\Pi$ ground state of C_6H. The estimated parameters in both $^2\Pi$ states of C_6D derived from this approximate R-T analysis are also summarized in Table II.

D. Excitation energy of the 11_1 $\mu^2\Sigma$ vibronic state

From the R-T analysis, the excitation energy of the lowest-lying 11_1 $\mu^2\Sigma$ vibronic state of C_6H is obtained as 10.7 ± 0.5 cm^{-1}. Additional measurements have been performed to experimentally determine the excitation energy of the 11_1 $\mu^2\Sigma$ vibronic state. This is accomplished by measuring a series of spectra with different rotational temperatures. For this a pinhole discharge nozzle is used, as described in the experimental section. The recorded spectra for the bands $[h_0]$, $[h_0']$, and $[h_1]$ are shown in Fig. 7. It is found that, with the ongoing adiabatic cooling the relative intensities of the bands $[h_0']$ and $[h_1]$ become smaller with respect to the band $[h_0]$. The relative intensities of the bands $[h_0']$ and $[h_1]$ are expressed by

$$\frac{I_{[h_0']}}{I_{[h_0]}} \sim \frac{N((0_0 + 11_2)^2\Pi_{1/2})}{N(0_0\ ^2\Pi_{3/2})} = \exp\left(-\frac{|A_0''|}{kT}\right) \tag{14}$$

$$\frac{I_{[h_1]}}{I_{[h_0]}} \sim \frac{N(11_1\,\mu^2\Sigma)}{N(0_0\ ^2\Pi_{3/2})} = \exp\left(-\frac{E(11_1\,\mu^2\Sigma)}{kT}\right) \tag{15}$$

where N is the population density of C_6H in separate low-lying vibronic levels, and T is the temperature (in Kelvin).

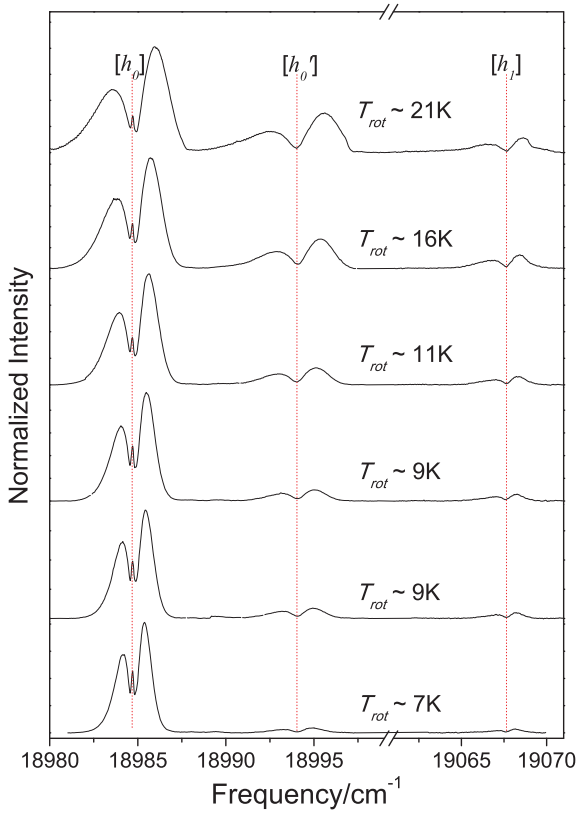

FIG. 7. Low resolution experimental spectra of the bands $[h_0]$, $[h_0']$, *and* $[h_1]$ with different rotational and vibrational temperatures through C/H plasma generated in a pinhole discharge nozzle.

As discussed in Sec. III C, the $0_0\ ^2\Pi_{1/2}$ level is significantly mixed with the $11_2\ ^2\Pi_{1/2}$ level. This mixing suggests that the C_6H populations in the three levels, $0_0\ ^2\Pi_{3/2}$, $(0_0+11_2)\ ^2\Pi_{1/2}$, and $11_1\ \mu^2\Sigma$, should be determined by the same effective vibronic temperature, i.e., the temperatures T in Eqs. (14) and (15) are most likely the same. Under this assumption,

$$\ln\left(\frac{I_{[h_1]}}{I_{[h_0]}}\right) = \frac{\mathrm{E}(11_1\ \mu^2\Sigma)}{|A_0|} * \ln\left(\frac{I_{[h_0']}}{I_{[h_0]}}\right) + \mathrm{C} \qquad (16)$$

applies, where C is a constant related to the Frank-Condon factors of the $0_0{}^0$ and $11_1{}^1$ transitions. In Fig. 8, a plot of relative intensities of the bands $[h_0']$ *vs* $[h_1]$ is shown, displaying a perfect linearity. The observation of this linearity provides proof for the validity of the assumption that spin and vibrational temperatures are equal. Using the value of $|A_0''| = 15.04\ \mathrm{cm}^{-1}$,[16] we obtain the excitation energy $E(11_1\ \mu^2\Sigma) \approx 11.4 \pm 0.5\ \mathrm{cm}^{-1}$, which is in reasonable agreement with the value resulting from the R-T analysis.

The final value for the excitation energy of the lowest-lying $11_1\ \mu^2\Sigma$ vibronic state is derived as average value from the experimental measurements and the R-T analysis, yielding $11.0 \pm 0.8\ \mathrm{cm}^{-1}$. This value is in agreement with the value of $\sim 14 \pm 7\ \mathrm{cm}^{-1}$ that was estimated previously from the microwave measurements,[19] but much more accurate.

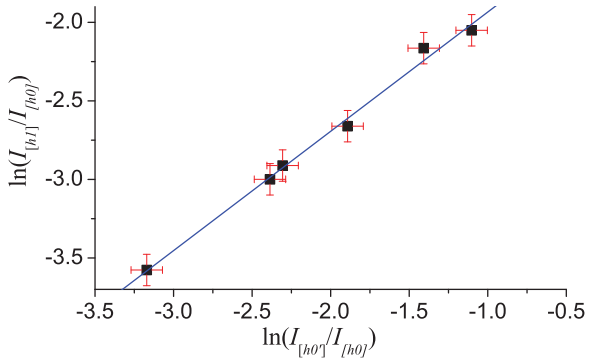

FIG. 8. The relative intensity of the bands $[h_1]$ and $[h_0']$ with respect to the band $[h_0]$. The uncertainty of the intensity determinations is estimated to be $\sim\pm 10\%$.

IV. DISCUSSION

The R-T analysis for the $X^2\Pi$ ground state results in a large value of the true SO coupling constant, $A_{SO}'' = -47\ \mathrm{cm}^{-1}$, which is much larger than the one-electron spin-orbit coupling constant for atomic carbon, $\zeta_C = 29\ \mathrm{cm}^{-1}$. In the $X^2\Pi$ ground state of HC_6H^+,[36,37] an ion isoelectronic with C_6H, the effective SO splitting constant $A_{eff}'' \sim -31\ \mathrm{cm}^{-1}$ is also larger than ζ_C. Such large SO coupling constants in long conjugated carbon chain systems cannot be explained based on the orbital approximation of LCAO (linear combination of atomic orbitals) theory. This means, that the LCAO approximation may become invalid for long conjugated $C_{2n}H$ systems. *Ab initio* calculations[32,38,39] show that dynamic electron correlation effects neglected in the LCAO approximation, are significant in the low-lying electronic states of the homologuous $C_{2n}H$ radicals and the HC_6H^+ ion. In addition, estimation of the SO coupling constants and hyperfine parameters by LCAO theory is usually applied for diatomic or tri-atomic molecules which can be simplified as a two-center system.[40] While the pattern of the conjugated Π bond in C_6H distributes along the molecular axis, it cannot be simplified as a two-center system. This may be another possible reason explaining why the LCAO approximation may become invalid for long $C_{2n}H$ radicals.

It is of interest to compare the values for the electronic SO coupling and R-T effect for the linear radicals C_4H and C_6H, which may reveal the behavior of angular momentum couplings in linear species with increasing chain length. Previous studies[15,16,34,38,39,41] show that the order of the first two electronic states, $X^2\Pi$ and $A^2\Sigma$ for C_6H, is reversed for the smaller species C_4H. The C_4H $A^2\Pi$ and C_6H $X^2\Pi$ states have a similar electronic configuration. As shown in Table III, the effective SO splitting constants (A_0) in the $X/A^2\Pi$ states and $B^2\Pi$ states of C_6H and C_4H are rather different. However, the values of the true SO coupling constants (A_{SO}) determined from the R-T analyses are very close for the two chains. Specifically, the A_{SO} values in both $^2\Pi$ states of C_6H are $\sim 5\%$ larger than those of C_4H. *Ab initio* calculations[32,38] have shown that conjugated Π bond systems become more stable with increasing the chain length of the homologues $C_{2n}H$ radicals. The slightly stronger electronic SO coupling in C_6H may arise from the higher stability of the conjugation in a longer chain.

From Table III, we also deduce that the coupling between the electronic orbital and CCC bending (ν_{11}) vibrational angular momenta in the $^2\Pi$ states of C_6H and C_4H must be rather different. For C_6H, the coupling between the CCC bending vibration (ν_{11}) and the $X^2\Pi$ electronic orbital motion is very strong (ε_{11} ~0.995), whereas it is much weaker in the $B^2\Pi$ state (ε_{11} ~0.089). In contrast, the couplings between the CCC bending vibration (ν_7) and both $^2\Pi$ states of C_4H are very weak (ε_7 ~0.016 and 0.061), but very strong for the CCH bending vibration (ν_6) in both $^2\Pi$ states (ε_6 ~0.99 and 0.656). For two members of the same linear chain family $C_{2n}H$, the lowest CCC bending vibrational modes are very similar. This suggests that, despite the fact that the lowest $(A/X)^2\Pi$ electronic states have the same open shell configuration, the electronic orbital motion may have changed from C_4H to C_6H, while in the second $B^2\Pi$ electronic state, the electronic orbital motion may be similar.

The present work also may have astronomical implications. In the R-T analysis of this work, contributions from other vibrational modes and intermode interactions are neglected. Since the parameter ε_{11} (~0.995) in the $X^2\Pi$ ground state of C_6H is large, it is expected that some other low-lying vibronic states exist that originate from combined vibrational excitation of ν_{11} and other bending modes, such as the CCH bending vibration. Such a complicated vibronic structure has been found in the $A^2\Pi$ state of C_4H.[34] Following the spectroscopic identifications of the 11_1 $\mu^2\Sigma$ and $^2\Delta$ vibronic states of C_6H, it was pointed out in Ref. 19 that there remain a number of unidentified features close in frequency to the identified C_6H rotational lines in both the laboratory plasma experiment and in the outer molecular envelope of IRC+10216. Some of these features, consequently, may be due to other low-lying vibronic states of C_6H. To reproduce the rotational structure in such vibronic states, a precise and comprehensive theoretical model, including R-T effect is needed.[40] Extending the laboratory work on the R-T effect to other vibrational modes of C_6H may help astronomers to assign the remaining unidentified C_6H features.

Since the electronic configuration and state order of C_6H and C_8H are the same, it is predicted that the true SO constant in the $X^2\Pi$ ground state of C_8H might be $A_{SO}'' \sim -50$ cm^{-1}, which is much larger than the effective SO splitting of $A_0'' \sim -19.3$ cm^{-1} determined from spectroscopic observation.[42,43] This large difference predicts a relatively large R-T effect (probably $\varepsilon > 0.9$) in the $X^2\Pi$ ground state of C_8H as well. On the other hand, as a longer chain, C_8H has more bending vibrational modes and a smaller vibrational energy for the CCC bending mode. As a consequence several vibronic states may lie very close to the 0_0 $^2\Pi_{3/2}$ ground level, as for C_6H but may exhibit a more complex structure. Up to now, both vibrationally excited C_4H and C_6H have been identified in IRC+10216,[18,44] as well as C_8H in its $X^2\Pi$ ground state.[45] It is very likely that vibrationally excited C_8H also exists in IRC+10216.

V. CONCLUSIONS

Rotationally resolved spectra of the $B^2\Pi$ - $X^2\Pi$ 0_0^0 electronic origin band and 11_1^1 $\mu^2\Sigma$ - $\mu^2\Sigma$ vibronic hot band transitions of both C_6H and C_6D are recorded by cavity ring-down spectroscopy, resulting in precise spectroscopic parameters. The Renner-Teller analysis indicates a large R-T interaction for the ν_{11} bending mode in the $X^2\Pi$ ground state of C_6H, and relatively small in the $B^2\Pi$ state. The excitation energy of the lowest-lying 11_1 $\mu^2\Sigma$ vibronic states is determined to be 11.0 ± 0.8 cm^{-1}.

ACKNOWLEDGMENTS

This work is financially supported by the Netherlands Foundation for Fundamental Research of Matter (FOM). The work has been performed within the context of the Netherlands Astrochemistry Network NWO program. Samples of C_2D_2 were generously made available by Professor Dr. S. Schlemmer (University of Cologne).

[1] H. Suzuki, M. Ohishi, N. Kaifu, S. Ishikaw, and T. Kasuga, Publ. Astron. Soc. Jpn. **38**, 911 (1986).
[2] J. Cernicharo, M. Guelin, K. M. Menten, and C. M. Walmsley, Astron. Astrophys. **181**, L1 (1987).
[3] J. C. Pearson, C. A. Gottlieb, D. R. Woodward, and P. Thaddeus, Astron. Astrophys. **189**, L13 (1988).
[4] N. Kaifu, M. Ohishi, K. Kawaguchi, S. Saito, S. Yamamoto, T. Miyaji, K. Miyazawa, S. Ishikawa, C. Noumaru, S. Harasawa, M. Okuda, and H. Suzuki, Publ. Astron. Soc. Jpn. **56**, 69 (2004).
[5] M. Guelin, J. Cernicharo, C. Kahane, J. Gomez-Gonzalez, and C. M. Walmsley, Astron. Astrophys. **175**, L5 (1987).
[6] S. Saito, K. Kawaguchi, H. Suzuki, M. Ohishi, N. Kaifu, and S. Ishikawa, Publ. Astron. Soc. Jpn. **39**, 193 (1987).
[7] K. Kawaguchi, Y. Kasai, S. Ishikawa, and N. Kaifu, Publ. Astron. Soc. Jpn. **47**, 853 (1995).
[8] J. Cernicharo, M. Guelin, and C. Kahane, Astron. Astrophys. Suppl. Ser. **142**, 181 (2000).
[9] J. P. Maier, Chem. Soc. Rev. **26**, 21 (1997).
[10] E. B. Jochnowitz, and J. P. Maier, Ann. Rev. Phys. Chem. **59**, 519 (2008).
[11] R. Nagarajan, and J. P. Maier, Int. Rev. Phys. Chem. **29**, 521 (2010).
[12] D. Forney, J. Fulara, P. Freicogel, M. Jakobi, D. Lessen, and J. P. Maier, J. Chem. Phys. **103**, 48 (1995).
[13] P. Freivogel, J. Fulara, M. Jakobi, D. Forney, and J. P. Maier, J. Chem. Phys. **103**, 54 (1998).
[14] M. Kotterer, and J. P. Maier, Chem. Phys. Lett. **266**, 342 (1997).
[15] T. R. Taylor, C. Xu, and D. M. Neumark, J. Chem. Phys. **108**, 10018 (1998).
[16] H. Linnartz, T. Motylewski, O. Vaizert, J. P. Maier, A. J. Apponi, M. C. McCarthy, C. A. Gottlieb, and P. Thaddeus, J. Mol. Spectrosc. **197**, 1 (1999).
[17] M. C. McCarthy, C. A. Gottlieb, H. Gupta, and P. Thaddeus, Astrophys. J. **652**, L141 (2006).
[18] J. Cernicharo, M. Guelin, M. Agundez, M. C. McCarthy, and P. Thaddeus, Astrophys. J. **688**, L83 (2008).
[19] C. A. Gottlieb, M. C. McCarthy, and P. Thaddeus, Astrophys. J. Suppl. **189**, 261 (2010).
[20] T. Motylewski, and H. Linnartz, Rev. Sci. Instrum. **70**, 1305 (1999).
[21] N. Wehres, D. Zhao, H. Linnartz, and W. Ubachs, Chem. Phys. Lett. **497**, 30 (2010).
[22] D. Zhao, N. Wehres, H. Linnartz, and W. Ubachs, Chem. Phys. Lett. **501**, 232–237 (2011).
[23] See supplementary material at http://dx.doi.org/10.1063/1.3609112 for the measured rotational transition frequencies of the observed bands in the present work.
[24] Rotational levels in the upper state of C_6D 0_0^0 electronic origin band are found to be heavily perturbed (see Table S2 in the supplementary material (Ref. 23)). In the least squares fit, the constant D' is set as D'' and fixed, and only levels with $J' \leq 15.5$ for the $\Omega = 3/2$ component and $J' \leq 10.5$ for the $\Omega = 1/2$ component are included to derive the spectroscopic constants T_0, B', A' and γ'. As a consequence, the rms of the fit and the resulted values of spectroscopic constants of C_6D are comparable to those of C_6H.
[25] PGOPHER, a Program for Simulating Rotational Structure, C. M. Western, University of Bristol, http://pgopher.chm.bris.ac.uk.

[26]C. A. Gottlieb, E. W. Gottlieb, and P. Thaddeus, Astron. Astrophys. **164**, L5 (1986).
[27]M. Tulej, F. J. Mazzotti, and J. P. Maier, J. Phys. Chem. A **115**, 6878 (2011).
[28]M. J. Travers, M. C. McCarthy, C. A. Gottlieb, and P. Thaddeus, Astrophysic. J. **465**, L77 (1996).
[29]J. T. Hougen, J. Chem. Phys. **36**, 519 (1962).
[30]J. M. Frye, and T. J. Sears, Mol. Phys. **62**, 919 (1987).
[31]S. T. Brown, J. C. Rienstra-Kiracofe, and H. F. Schaefer, III, J. Phys. Chem. A **103**, 4065 (1999).
[32]Z. Cao, and S. P. Peyerimho, Phys. Chem. Chem. Phys. **3**, 1403 (2001).
[33]Y. Wu, Comput. Theor. Chem. **963**, 104 (2011).
[34]F. J. Mazzotti, R. Raghunandan, A. M. Esmail, M. Tulej, and J. P. Maier, J. Chem. Phys. **134**, 164303 (2011).
[35]G. Herzberg, *Molecular Spectra and Molecular Structure III. Electronic Spectra and Electronic Structure of Polyatomic Molecules* (D. Van Nostrand, New York, 1966).
[36]W. E. Sinclair, D. Pfluger, H. Linnartz, J. P. Maier, J. Chem. Phys. **110**, 296 (1999).
[37]D. Pfluger, W. E. Sinclair, H. Linnartz, J. P. Maier, Chem. Phys. Lett. **313**, 171 (1999).
[38]A. L. Sobolewski, and L. Adamowicz, J. Chem. Phys. **102**, 394 (1995).
[39]D. E. Woon, Chem. Phys. Lett. **244**, 45 (1995).
[40]M. D. Allen, K. M. Evenson, D. A. Gillett, and J. M. Brown, J. Mol. Spectrosc. **201**, 18 (2000).
[41]K. Hoshina, H. Kohguchi, Y. Ohshim, and Y. Endo, J. Chem. Phys. **108**, 3465 (1998).
[42]M. C. McCarthy, M. J. Travers, A. Kovacs, C. A. Gottlieb, and P. Thaddeus, Astron. Astrophys. **309**, L31 (1996).
[43]H. Linnartz, T. Motylewski, and J. P. Maier, J. Chem. Phys. **109**, 3819 (1998).
[44]M. Guelin, J. Cernicharo, S. Navarro, D. R. Woodward, C. A. Gottlieb, and P. Thaddeus, Astron. Astrophys. **182**, L37 (1987).
[45]J. Cernicharo, and M. Guelin, Astron. Astrophys. **309**, L27 (1996).